Decoherence of quantum superpositions through coupling to engineered reservoirs

C. J. Myatt*, B. E. King*, Q. A. Turchette, C. A. Sackett, D. Kielpinski, W. M. Itano, C. Monroe & D. J. Wineland

National Institute of Standards and Technology, Div. 847.10, 325 Broadway, Boulder, Colorado 80303, USA

The theory of quantum mechanics applies to closed systems. In such ideal situations, a single atom can, for example, exist simultaneously in a superposition of two different spatial locations. In contrast, real systems always interact with their environment, with the consequence that macroscopic quantum superpositions (as illustrated by the 'Schrödinger's cat' thought-experiment) are not observed. Moreover, macroscopic superpositions decay so quickly that even the dynamics of decoherence cannot be observed. However, mesoscopic systems offer the possibility of observing the decoherence of such quantum superpositions. Here we present measurements of the decoherence of superposed motional states of a single trapped atom. Decoherence is induced by coupling the atom to engineered reservoirs, in which the coupling and state of the environment are controllable. We perform three experiments, finding that the decoherence rate scales with the square of a quantity describing the amplitude of the superposition state.

One of the fundamental properties of quantum mechanics is the principle of superposition, a principle whose introduction was considered a "drastic" measure by Dirac[1]. The fact that quantum superpositions do not exist in the macroscopic world hinders our intuition and leads to the apparently strange behaviour dictated by quantum mechanics. A famous example of this was posed by Schrödinger in 1935 (ref. 2) who pointed out that quantum mechanics would predict bizarre situations such as a cat being simultaneously dead and alive. The existence of superpositions prescribed by quantum mechanics is valid for systems that are closed, that is, free from external influences. In contrast, real systems always couple to these external influences, the environment, which is typically composed of an extremely large number of degrees of freedom. Lack of knowledge about the environment is expressed by averaging (mathematically tracing) over the possible states of the environmental degrees of freedom. This leads to an evolution of the density matrix of the system, in which the quantum superpositions are continuously reduced to classical probability distributions, a process generally known as decoherence (see, for example, refs 3–5). One approach to describing decoherence is to treat the environment as a reservoir of quantum oscillators, each of which interacts with the quantum system in question. An example of such a reservoir–system interaction is the ensemble of empty electromagnetic field modes, each represented by a quantized harmonic oscillator, interacting with an atom in order to induce spontaneous emission. As a quantum superposition is made larger, decoherence tends to act more quickly. For truly macroscopic superpositions, such as that of 'Schrödinger's cat', decoherence occurs on such a short timescale that it is almost impossible to observe quantum coherences. However, mesoscopic systems present the possibility of studying, in a controlled way, the process of decoherence and the transition from quantum to classical behaviour.

In the past few years, techniques have been realized to generate mesoscopic superpositions, also called 'Schrödinger cats', of motional states of trapped ions[6] and of photon states in the context of cavity QED (ref. 7), where decoherence through coupling to ambient reservoirs and the sensitivity of the rate of decoherence to the size of cat were observed. Here we extend the investigations beyond the ambient reservoirs and 'engineer' the state of the reservoir, as well as the form of the system–reservoir coupling. One way this can be achieved for a system of trapped ions is by applying noisy potentials to the trap electrodes, simulating a hot resistor (reservoir) connected to the trap electrodes, with controllable temperature and spectrum. For a range of two-component superposition states, we demonstrate the expected exponential dependence of the decoherence rate on the separation of the components in Hilbert space. We also present the first, to our knowledge, study of decoherence into an engineered quantum reservoir, using laser cooling techniques to generate an effectively zero-temperature bath[8,9].

Theoretical predictions

Decoherence of specific mesoscopic quantum superpositions, with a variety of couplings to a reservoir, has been investigated extensively in theory[3–5,8,10–12]. The model in these studies is a system harmonic oscillator coupled to a bath of environment quantum oscillators. (These and other sources of decoherence in the context of trapped-ion experiments have been more recently discussed theoretically in refs 13–16.) As an illustration, we consider the system oscillator to be in a superposition of coherent states. A coherent state[17] of a harmonic oscillator is a gaussian wavepacket which oscillates back and forth while retaining its shape. In quantum mechanics, a coherent state is represented by a state vector $|\alpha\rangle$, where $\alpha = |\alpha|e^{i\theta}$ is a complex number whose magnitude $|\alpha|$ is a dimensionless amplitude of the wavepacket's motion and whose phase θ is the phase of the oscillation at some initial time $t = 0$ (the phases of all subsequent coherent manipulations are set relative to this initial phase). Coherent states are analogous to classical trajectories of a harmonic oscillator, approximated by a marble rolling back and forth in a bowl. A superposition of coherent states, $|\psi\rangle = N(|\alpha_1\rangle + |\alpha_2\rangle)$ where N is a normalization factor, can be visualized as a marble rolling in a superposition of two trajectories.

We consider the system oscillator to couple to the reservoir through an interaction proportional to the product of the amplitude of motion of the system oscillator and the amplitude of

* Present addresses: Research Electro-Optics, 1855 South 57th Court, Boulder, Colorado 80301, USA (C.J.M.); NIST, Atomic Physics Division (842), 100 Bureau Drive, Stop 8424, Gaithersburg, Maryland 20899-8424, USA (B.E.K.).

fluctuations of the reservoir. For brevity, we call this an amplitude reservoir. In the classical analogy, a hot amplitude reservoir behaves as if the bowl is subject to random displacements of its centre, resulting in a random force on the marble. For a superposition of coherent states coupled to such a reservoir, a simple scaling law may be stated: the rate of decoherence (here a dephasing between the $|\alpha_1\rangle$ and $|\alpha_2\rangle$ components of $|\psi\rangle$) scales as the square of the separation of the wave packets, $|\alpha_1 - \alpha_2|^2$. In an idealized case where, first, the superposition is created, then the amplitude reservoir is coupled to the system for a time t, and then the coupling is turned off, the remaining coherence between the two wave packets is[4]:

$$C(t) = \exp[-|\alpha_1 - \alpha_2|^2 \xi t] \quad (1)$$

Here ξ is a coupling constant between the reservoir and the system. The larger the size ($|\alpha_1 - \alpha_2|$) of the superposition, the faster the decoherence.

Another basis of quantum states for the harmonic oscillator is the energy eigenstates, also known as Fock or number states. The Fock state $|n\rangle$ has energy $\hbar\omega(n + 1/2)$ and represents a state of n units of quantized vibration, where $n \geqslant 0$ is an integer. Fock states have no classical analogue, as they are delocalized in position and uniformly distributed in phase. A superposition of two Fock states $|\psi\rangle = (|n_1\rangle + |n_2\rangle)/\sqrt{2}$ loses coherence when the modes of the reservoir couple linearly to the energy of the oscillator, which is equivalent to averaging over a gaussian distribution of phase shifts of the oscillator. We denote this case a phase reservoir. The coherence between the two Fock states decays at a rate that scales as the square of the difference between the Fock indices, $|n_1 - n_2|^2$, given by[4]:

$$C(t) = \exp[-|n_1 - n_2|^2 \kappa t] \quad (2)$$

Here κ is a coupling constant.

Trapped ions

In the experiments described here, a linear Paul trap, similar to the one described in ref. 18, confines single $^9Be^+$ atomic ions in a harmonic potential, for which we isolate the axial motion at frequency $\omega = 2\pi \times 11.3$ MHz. Within the ion's electronic ground-state hyperfine manifold we restrict our attention to two states, the $|F = 2, m_F = -2\rangle$ state, which we label $|\downarrow\rangle$, and the $|F = 1, m_F = -1\rangle$ state, which we label $|\uparrow\rangle$, separated in energy by $\hbar\omega_0$, where $\omega_0 \approx 2\pi \times 1.25$ GHz, and where F and m_F are the quantum numbers associated with the total angular momentum of the atomic state. The ion is cooled to the $n = 0$ ground state of motion, denoted $|0\rangle$, and optically pumped to the $|\downarrow\rangle$ state with resolved-sideband stimulated Raman cooling[19]. Thus, the initial state for all the experiments is $|\downarrow\rangle|0\rangle$.

We drive coherent stimulated Raman transitions with a pair of laser beams detuned approximately 12 GHz from the atomic resonance near 958 THz ($\lambda = 313$ nm). We use three types of Raman transitions, determined by the beam geometry and difference frequency of the two beams: (1) Motion-independent spin-flip transitions ($|\downarrow\rangle|n\rangle \leftrightarrow |\uparrow\rangle|n\rangle$). Here, the Raman beams are co-propagating and the difference frequency is set to ω_0. (2) Sideband transitions ($|\downarrow\rangle|n\rangle \leftrightarrow |\uparrow\rangle|n + \Delta n\rangle$). Here, the beams are orientated with their difference wavevector pointing along the trap axis and their difference frequency set to a motional sideband at $\omega_0 + \omega\Delta n$. (3) Motional displacement transitions. Here, the beams are orientated with their difference wavevector pointing along the trap axis and their difference frequency set to the trap frequency ω. This approximates the harmonic-oscillator displacement operator $D(\alpha)$, where the operator is defined[4,5] by the relation $D(\alpha)|0\rangle = |\alpha\rangle$. The displacement $|\alpha|$ is proportional to the duration of the laser pulse, and θ is set by the phase of the applied laser field[6,13]. In general, α depends on the internal state of the ion.

We can efficiently detect the $|\downarrow\rangle$ internal state of the ion by applying circularly polarized laser light resonant with the transition $|\downarrow\rangle \leftrightarrow |e\rangle$, where $|e\rangle$ is a short-lived excited electronic state that usually decays back to $|\downarrow\rangle$ by emitting a photon[19]. In contrast, the transition $|\uparrow\rangle \leftrightarrow |e\rangle$ is out of resonance, and an ion in the $|\uparrow\rangle$ state scatters negligible light.

High-temperature amplitude reservoir

The motion of a trapped ion couples to uniform electric fields $\mathbf{E}$ through the potential $U = -q\mathbf{x} \cdot \mathbf{E}$, where $\mathbf{x}$ is the displacement of the ion from its equilibrium position (proportional to the amplitude of motion) and q is the charge of the ion. This coupling is independent of the ion's internal state. Our engineered amplitude reservoir consists of random uniform electric fields applied along the axis of the trap, oscillating near the ion's axial-motion frequency ω. We generate axial fields in the trap by applying voltages to one of the trap electrodes. A commercial function generator produces

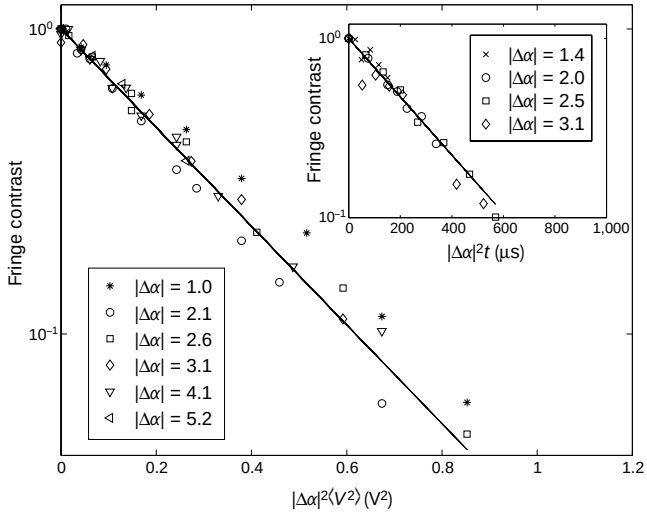

Figure 1 The decoherence of 'Schrödinger-cat' states coupled to an amplitude reservoir. In the main figure, each point is the measured contrast of the interference fringes after noisy potentials were applied to the trap electrodes. The fringe contrast at $\langle V^2\rangle = 0$ is scaled to unity in order to make comparisons between different values of $|\Delta\alpha|$. The size of the superposition, $|\Delta\alpha|$, varies linearly with the pulse time for Raman transition type (3). The applied mean-squared voltage $\langle V^2\rangle$ is scaled by $|\Delta\alpha|^2$. The solid line is a fit to an exponential. Inset, fringe contrast versus time of interaction with ambient fields is plotted. Again, the fringe contrast is scaled to unity at $t = 0$ for comparison between different values $|\Delta\alpha|$. The solid line is a fit to an exponential.

pseudo-random voltages which are applied through a band-pass filter centred near ω, defining the frequency spectrum of the reservoir.

In all the experiments reported here, we measure the coherence of the quantum superpositions with single-atom interferometry, analogous to that used in our previous work[6]. For example, to observe the effects of the amplitude reservoir, the motional state of the ion is split into a superposition of two components, each associated with a different internal state of the ion, forming a state like that of the Schrödinger cat[6]. The superposition is then coupled to the reservoir, and finally the perturbed superposition is recombined by reversing the steps which initially created it. We repeat the experiment many times, measuring the internal state of the ion as a function of the relative phase of the creation and reversal steps, and the contrast of the resulting interference fringes characterizes the amount of coherence remaining after coupling to the reservoir.

In more detail, we first form a cat state of the form:

$$|\psi_c\rangle = (|\downarrow\rangle|\alpha_\downarrow\rangle + |\uparrow\rangle|\alpha_\uparrow\rangle)/\sqrt{2} \quad (3)$$

This is created by driving a Raman transition (type (1)) to generate an equal spin superposition, $|\downarrow\rangle|0\rangle \rightarrow (|\downarrow\rangle + |\uparrow\rangle)|0\rangle/\sqrt{2}$, followed by a Raman transition (type (3)), with laser polarizations set such that $\alpha_\uparrow = -\alpha_\downarrow/2$ in equation (3).

A uniform electric field oscillating near the trap frequency ω (applied in the experiment for 3 μs) results in the displacement operator $D(\beta)$ acting equally on both $|\downarrow\rangle$ and $|\uparrow\rangle$, giving:

$$|\psi_c\rangle \rightarrow |\psi_c'\rangle = (|\downarrow\rangle|\beta + \alpha_\downarrow\rangle + e^{i\phi_m}|\uparrow\rangle|\beta + \alpha_\uparrow\rangle)/\sqrt{2} \quad (4)$$

Here $\phi_m = \mathrm{Im}\beta\Delta\alpha^*$ and $\Delta\alpha = \alpha_\downarrow - \alpha_\uparrow$. We probe the coherence by reversing the steps taken to generate the cat state. We first reverse the motional Raman transition (type (3)), resulting in the state

$$|\psi_c'\rangle \rightarrow |\psi''\rangle = (|\downarrow\rangle + e^{2i\phi_m}|\uparrow\rangle)|\beta\rangle/\sqrt{2} \quad (5)$$

A final pulse on the motion-independent spin-flip transition (1), with phase δ relative to the first pulse on transition (1), leads to interference fringes with a residual phase shift $2\phi_m$. Averaging over the gaussian random variable β, the probability of finding the ion in the $|\downarrow\rangle$ state is[21]:

$$P_\downarrow = \frac{1}{2}(1 - e^{-2|\Delta\alpha|^2\sigma^2}\cos\delta) \quad (6)$$

Interference fringes are generated by recording $P_\downarrow$ while sweeping δ. The variance σ^2 of β is proportional to the mean-squared voltage noise $\langle V^2\rangle$ (proportional to the temperature of the simulated resistor). A plot of the interference-fringe contrast as a function of the applied mean-squared voltage, scaled by the squared 'size' of the cat state $|\Delta\alpha|^2$, is shown in Fig. 1. Decay curves were recorded for a variety of superposition sizes $|\Delta\alpha|$, and all the data agree with a single exponential.

In addition to the engineered reservoir of the applied voltage noise, the ion also interacts with ambient fluctuating electric fields, which we expect to have the character of an amplitude reservoir. To examine this 'natural' decoherence, we ran the experiment outlined above without any applied voltage noise, and with a variable time t between the creation of the cat state and the recombination. The fringe visibility as a function of $|\Delta\alpha|^2 t$ is shown in the inset to Fig. 1. The decay curves are normalized to unity at $t = 0$. The decay of the fringe visibility is exponential, and the decay constant $\gamma \approx 6.7 \times 10^{-3}\ \mu s^{-1}$ is consistent with the measured heating rate[13] of $\gamma \approx 5.9 \times 10^{-3}\ \mu s^{-1}$ for this apparatus. The effects of this ambient reservoir were negligible during the time (3 μs) that the engineered amplitude reservoir was coupled to the ion.

High-temperature phase reservoir

A phase reservoir coupled to the ion is simulated by random variations in the trap frequency ω, changing the phase of the ion oscillation without changing its energy. We realize this coupling experimentally by modulating the trap frequency. A random voltage noise source is passed through a low-pass filter network with a cut-off frequency well below ω to maintain adiabaticity. The fluctuations in potential are applied symmetrically to the trap electrodes so as to produce linear field gradients and negligible uniform fields. This in turn perturbs the trap frequency, by $\delta\omega(t)$. When integrated over the time (20 μs) of the applied noise, the ion's motion is phase-shifted by $\phi = \int\delta\omega(t)\mathrm{d}t$. This technique yields a gaussian-distributed ensemble of phase shifts with variance σ^2 proportional to the applied mean-squared voltage noise $\langle V^2\rangle$.

Motional decoherence caused by a phase reservoir is clearly illustrated with a superposition of two Fock states. We generate superpositions of Fock states of the form $|\psi\rangle = |s\rangle(|n\rangle + |n'\rangle)/\sqrt{2}$, where $s = \downarrow$ or $\uparrow$, with pulses on the Raman motional sidebands (case (2) above) as in ref. 20. The trap frequency is then perturbed by the

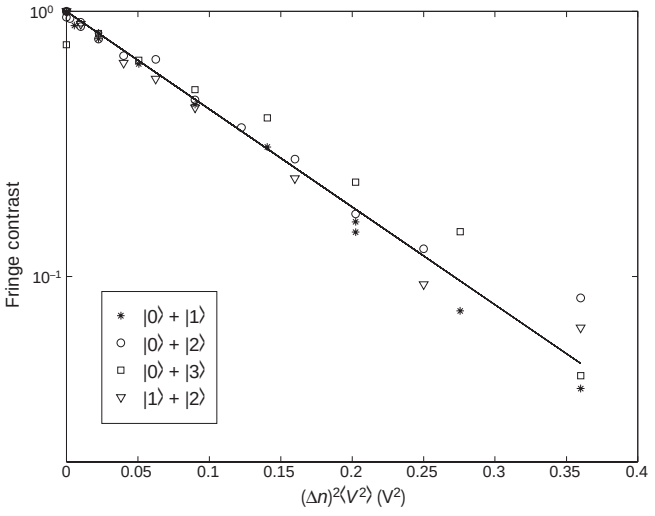

Figure 2 Decoherence of superpositions of Fock states coupled to the phase reservoir. The data points are the measured fringe contrast. The fringe contrast is normalized to unity at $\langle V^2\rangle = 0$. The mean squared voltage applied to the trap electrodes is scaled by the squared size of the superposition $|\Delta n|^2$. The solid line is a fit to an exponential.

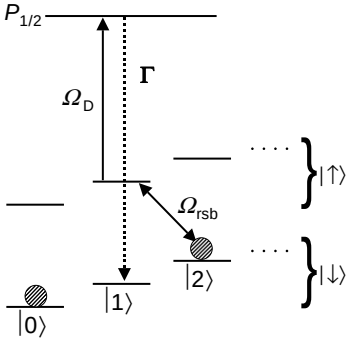

Figure 3 Implementation of an engineered zero-temperature reservoir. The states $|\downarrow\rangle|n\rangle$ and $|\uparrow\rangle|n-1\rangle$ are coupled by driving Raman motion-sensitive transitions (case (2) in the text). The state $|\uparrow\rangle$ is coupled to the environment by applying a weak optical pumping beam. The circles represent the superposition generated before applying this zero-temperature reservoir. The arrows show how the population in the $|\downarrow\rangle|2\rangle$ state is driven to the $|\uparrow\rangle|1\rangle$ state, and subsequently to the $|\downarrow\rangle|1\rangle$ state, through spontaneous Raman scattering.

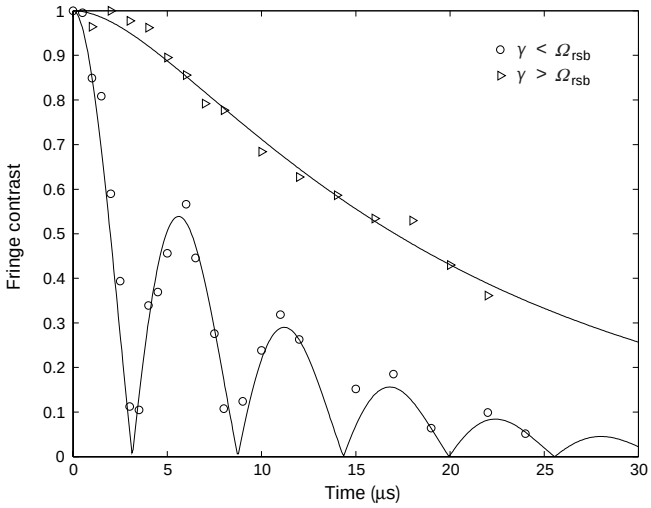

Figure 4 Decoherence of a Fock state superposition into the engineered zero-temperature reservoir. Fringe contrast is plotted as a function of the time the system is coupled to the zero temperature reservoir. The only difference in the two cases shown was the intensity of the optical pumping beam (see Fig. 3).

applied random potentials, and the Fock states of the superposition acquire a relative phase factor $e^{i\psi\Delta n}$, where $\Delta n = n - n'$. The steps that created the superposition are then reversed, with a relative phase difference δ between the creation and reversal pulses, leading to a probability of detecting the ion in the $|\downarrow\rangle$ state[21]:

$$P_{\downarrow} = \frac{1}{2}[1 + e^{-|\Delta n|^2\sigma^2/2}\cos\delta] \qquad (7)$$

Interference fringes are recorded by varying δ as in the Schrödinger-cat interferometer. The fringe contrast is plotted as a function of $|\Delta n|^2\langle V^2\rangle$ in Fig. 2. As with the Schrödinger-cat states and amplitude reservoir, the data were fitted by a single exponential in $|\Delta n|^2\langle V\rangle^2$.

Zero-temperature reservoir

A third type of engineered reservoir requires a quantum mechanical description. This is a bath of laser cooling light plus optical spontaneous emission, an engineered (nearly) zero-temperature reservoir following the suggestion of Poyatos *et al.*[8]. Our implementation, shown in Fig. 3, is essentially a continuous Raman cooling technique. A pair of Raman beams (case (2)), tuned to the first red sideband, couples the states $|\downarrow\rangle|n\rangle \leftrightarrow |\uparrow\rangle|n-1\rangle$. Concurrently, an optical pumping beam causes spontaneous Raman transitions from $|\uparrow\rangle$ to $|\downarrow\rangle$ through an unstable excited state $|e\rangle$, which decays at rate Γ. The Raman coupling strength is characterized by the Rabi frequency $\Omega_{\rm rsb}$, a function of the intensity and detuning of the Raman beams[13]. If the Rabi frequency of the optical pumping beam is $\Omega_{\rm D}$, then we can define an effective damping rate for the $|\uparrow\rangle$ state of $\gamma = \Omega_{\rm D}^2/\Gamma$, valid for our case of $\Omega_{\rm D} \ll \Gamma$. From the diagram in Fig. 3 we see that all populations are driven towards the state $|\downarrow\rangle|0\rangle$, the defining property of a zero-temperature reservoir. By varying the strength of the Raman and optical pumping couplings, we can control the reservoir parameters.

In the experiment, we examine the time evolution of the coherence of the Fock state superposition $\psi = |\downarrow\rangle(|0\rangle + |2\rangle)/\sqrt{2}$ for varying lengths of reservoir-interaction time. The interferometry is the same as in the study of the phase reservoir, where the Fock superposition is created, coupled to the reservoir, recombined, and probed, generating interference fringes. The data are shown in Fig. 4. Each data point represents the contrast of the fringes after the system interacts with the reservoir. We show two cases, $\gamma < \Omega_{\rm rbs}$ and $\gamma > \Omega_{\rm rsb}$. In the former case, the coherence between the $|0\rangle$ and $|2\rangle$ state disappears and reappears over time, with an overall decay of the fringe contrast. The underlying effect is population transfer back and forth (Rabi flopping) between the states $|\downarrow\rangle|2\rangle$ and $|\uparrow\rangle|1\rangle$ with a coupling of the $|\uparrow\rangle|1\rangle$ state to the outside environment through spontaneous Raman scattering. In effect, we have restricted the size of the environment (here the manifold of $|\uparrow\rangle|n\rangle$ states, weakly coupled to the outside environment) to an extent where we can reverse the effects of decoherence (of the $\psi = |\downarrow\rangle(|0\rangle + |2\rangle)/\sqrt{2}$ state) in a way similar to that proposed in ref. 22. This is also a striking example of non-exponential decay[23] in a context that is investigated in ref. 24. For the case $\gamma > \Omega_{\rm rsb}$, the fringe contrast decreases monotonically to zero. Even in the case of monotonic decay, a deviation from exponential is observed, a manifestation of the quantum Zeno effect[24,25].

Although the data with $\gamma < \Omega_{\rm rsb}$ illustrate how coherence transferred to the environment can be recovered, an alternative explanation would say that by transferring the $|\downarrow\rangle|2\rangle$ component of the superposition to the $|\uparrow\rangle|1\rangle$ state, we gain 'which-path' information in our interferometer—the paths being the $|\downarrow\rangle|0\rangle$ and $|\downarrow\rangle|2\rangle$ parts of the superposition. The oscillation in which-path information is analogous to that illustrated by other experiments[26,27].

Conclusions

The decoherence caused by the engineered high-temperature reservoirs described above can be explained by ensemble-averaging over random classical fields applied to the ion[21,28]. From previous experiments[20], we know that we can undo the effects of this decoherence by applying, in each experiment, a pulse of radiation that reverses the 'random' displacement. Similarly, the experiments here could also be carried out by coupling a hot resistor (with appropriate spectral filtering) between the trap electrodes (our case would correspond to a limit where the temperature $T \to \infty$ and the damping resistance $R \to 0$) (ref. 10). However, even in this case we could, subject to both practical and fundamental measurement uncertainties, record the voltages applied to the electrodes and reverse the effects of the random noise in each experiment. If we choose to ignore any knowledge of the electrical potentials applied to the trap electrodes, we can account for the observations just as well by considering the ion to be coupled to a large number of quantum oscillators, forming a heat bath. In the latter case, the state of the ion is entangled with that of the environment oscillators. After tracing over the environment variables, we are left with a reduced system, involving only the ion. The behaviour is the same as that obtained in the former case, in which the decoherence is caused by a deliberately applied external potential, but the environment is not considered to be a dynamical system itself[3,4]. Loosely speaking, the effect of an environment oscillator in the latter case is replaced by that of a single Fourier component of the electrical potential in the former case. Therefore, in the high-temperature limit simulated

by the first two experiments, one need not consider the entanglement with the environment because the environment noise can be sensed (classically) and its effects reversed. This is in contrast to the decay of ion motion into a zero-temperature reservoir described above, similar to that seen in cavity-QED experiments[7]. In this case, after the quantum system couples to the environment through spontaneous emission, a measurement of the environment is not sufficient to reverse the effects of decoherence.

The methods of engineering reservoirs that are presented here begin to broaden the field of experimental investigations of decoherence. With control over the reservoir parameters combined with non-classical motional states of trapped ions, detailed comparisons between theory and experiment are possible. Here we have simulated the decoherence caused by coupling a charged atom to a hot resistor (reservoir) by applying noisy voltages to the ion-trap electrodes. The cases considered demonstrate a quadratic dependence of the rate of decoherence on the size of the superpositions, demonstrating the difficulty in generating truly macroscopic superpositions, such as that of 'Schrödinger's cat'. As a practical matter, these 'high-temperature' sources of noise are important because they currently limit the performance of a trapped-ion quantum computer[13]. We have also simulated a zero-temperature reservoir by using laser cooling to damp the ion motion. Extensions of the technique used to generate this zero-temperature bath should permit some interesting system–bath interactions that would be difficult to realize in any other way. One possibility is generating a squeezed reservoir, where all initial states asymptotically relax to a squeezed state of motion[8]. Other couplings can be tailored to relax the system into a 'Schrödinger-cat' state[29,30]. □

Received 24 September; accepted 30 November 1999.

1. Dirac, P. A. M. *The Principles of Quantum Mechanics* (Oxford Univ. Press, Clarendon, 1958).
2. Schrödinger, E. Die gegenwärtige situation in der quantenmechanik. *Naturwissenschaften* **23,** 807–812, 823–828, 844–849 (1935).
3. Zurek, W. H. Decoherence and the transition from quantum to classical. *Phys. Today* **44,** 36–44 (1991).
4. Walls, D. F. & Milburn, G. J. *Quantum Optics* (Springer, Berlin, 1994).
5. Bužek, V. & Knight, P. L. Quantum interference, superposition states of light, and nonclassical effects. *Prog. Opt.* **XXXIV,** 1–158 (1995).
6. Monroe, C., Meekhof, D. M., King, B. E. & Wineland, D. J. A "Schrödinger cat" superposition state of an atom. *Science* **272,** 1131–1136 (1996).
7. Brune, M. *et al.* Observing the progressive decoherence of the "meter" in a quantum measurement. *Phys. Rev. Lett.* **77,** 4887–4890 (1996).
8. Poyatos, J. F., Cirac, J. I. & Zoller, P. Quantum reservoir engineering with laser cooled trapped ions. *Phys. Rev. Lett.* **77,** 4728–4731 (1996).
9. Marzoli, I., Cirac, J. I., Blatt, R. & Zoller, P. Laser cooling of trapped three-level ions: designing two-level systems for sideband cooling. *Phys. Rev. A* **49,** 2771–2779 (1994).
10. Caldeira, A. O. & Leggett, A. J. Influence of damping on quantum interference: an exactly soluble model. *Phys. Rev. A* **31,** 1059–1066 (1985).
11. Walls, D. F. & Milburn, G. J. Effect of dissipation on quantum coherence. *Phys. Rev. A* **31,** 2403–2408 (1985).
12. Collett, M. J. Exact density-matrix calculations for simple open systems. *Phys. Rev. A* **38,** 2233–2247 (1988).
13. Wineland, D. J. *et al.* Experimental issues in coherent quantum-state manipulations of trapped atomic ions. *J. Res. NIST* **103,** 259–328 (1998).
14. Schneider, S. & Milburn, G. J. Decoherence in ion traps due to laser intensity and phase fluctuations. *Phys. Rev. A* **57,** 3748–3752 (1998).
15. Murao, M. & Knight, P. L. Decoherence in nonclassical motional states of a trapped ion. *Phys. Rev. A* **58,** 663–669 (1998).
16. Schneider, S. & Milburn, G. J. Decoherence and fidelity in ion traps with fluctuating trap parameters. *Phys. Rev. A* **59,** 3766–3774 (1999).
17. Glauber, R. J. Coherent and incoherent states of the radiation field. *Phys. Rev.* **131,** 2766–2788 (1963).
18. Raizen, M. G., Gilligan, J. M., Bergquist, J. C., Itano, W. M. & Wineland, D. J. Ionic crystals in a linear Paul trap. *Phys. Rev. A* **45,** 6493–6501 (1992).
19. Monroe, C. *et al.* Resolved-sideband Raman cooling of a bound atom to the 3D zero-point energy. *Phys. Rev. Lett.* **75,** 4011–4014 (1995).
20. Meekhof, D. M., Monroe, C., King, B. E., Itano, W. M. & Wineland, D. J. Generation of nonclassical motional states of a trapped atom. *Phys. Rev. Lett.* **76,** 1796–1799 (1996).
21. Myatt, C. J. *et al.* in *Laser Spectroscopy 13* (ed. Blatt, R., Eschner, J., Leibfried, D. & Schmidt-Kaler, F.) (World Scientific, Singapore, in the press).
22. Raimond, J. M., Brune, M. & Haroche, S. Reversible decoherence of a mesoscopic superposition of field states. *Phys. Rev. Lett.* **79,** 1964–1967 (1997).
23. Wilkinson, S. R. *et al.* Experimental evidence for non-exponential decay in quantum tunnelling. *Nature* **387,** 575–577 (1997).
24. Thompson, R. C., Hernandez-Pozos, J.-L., Höffges, J., Segal, D. M. & Vincent, J. R. in *Trapped Charged Particles and Fundamental Physics* (eds Dubin, D. H. E. & Schneider, D.) 388–392 (American Institute of Physics Conf. Proc. 457, AIP Press, Woodbury, New York, 1999).
25. Itano, W. M., Heizen, D. J., Bollinger, J. J. & Wineland, D. J. Quantum Zeno effect. *Phys. Rev. A* **41,** 2295–2300 (1990).
26. Chapman, M. S. *et al.* Photon scattering from atoms in an interferometer: coherence lost and regained. *Phys. Rev. Lett.* **75,** 3783–3787 (1995).
27. Dürr, S., Nonn, T. & Rempe, G. Fringe visibility and which-way information in an atom interferometer. *Phys. Rev. Lett.* **81,** 5705–5709 (1998).
28. Itano, W. M. *et al.* Quantum harmonic oscillator state synthesis and analysis. *Proc. SPIE* **2995,** 43–55 (1997).
29. de Matos Filho, R. L. & Vogel, W. Even and odd coherent states of the motion of a trapped ion. *Phys. Rev. Lett.* **76,** 608–611 (1996).
30. Garraway, B. M., Knight, P. L. & Plenio, M. B. Generation and preservation of coherence in dissipative quantum optical environments. *Phys. Scr.* **T76,** 152–158 (1998).

Acknowledgements

We thank the US National Security Agency, Army Research Office, and Office of Naval Research for support. We thank P. Zoller, H. Mabuchi and W. Zurek for discussions. We thank them, D. Leibfried, M. Rowe, D. Sullivan and M. Lombardi for comments on the manuscript.

Correspondence and requests for materials should be addressed to D.J.W. (e-mail: dwineland@nist.gov).